Carbonates Evaporites (2012) 27:71–85
DOI 10.1007/s13146-012-0085-6

ORIGINAL ARTICLE

Activity diagrams of borates: implications on common deposits

Rezan Birsoy · Ünal Özbaş

Accepted: 24 January 2012 / Published online: 15 February 2012
© Springer-Verlag 2012

Abstract Most of the world's borate minerals are found in Neogene deposits and Quaternary lake deposits. Only a few of the borates are common geologically and commercially. A series of equilibrium activity diagrams were calculated for the common as well as some rare borate minerals in the systems of (1) Na_2O–B_2O_3–H_2O, (2) CaO–B_2O_3–H_2O ± CO_2, (3) MgO–B_2O_3–H_2O ± CO_2, (4) CaO–Na_2O–B_2O_3–H_2O, and (5) CaO–MgO–B_2O_3–H_2O. Stability diagrams constructed with respect to variables of $\log[a_{Mb^{n+}}/(a_{H^+})^n]$ and $\log[a_{Mb^{n+}}/a_{Mc^{(n-1)+}}(a_{H^+})]$ versus both $\log[a_{H_2O}]$ and $\log[a_{B(OH)_3}]$ showed that some rare borates are thermodynamically not stable (tertschite, inderborite) at all in these systems. Still some common phases are thermodynamically occurred as metastable phases (tincalconite, meyerhofferite) in some deposits. On the contrary, some thermodynamically stable phases can form kinetically slower than the others and not found as common phases (inyoite). Some common and uncommon minerals such as ulexite, aksaite, and gowerite have small stability fields indicating that they can form at very limited thermodynamic conditions. Some phases such as pandermite, ginorite, ascharite, and suanite being structurally complex phases, form after less complex precursor minerals at the end of diagenesis due to burial and/or increasing temperature. Concentrations of cations and boron, pH, evaporation rate are other controlling variables of diagenetic processes. Through these diagrams, observed paragenetic relations and geochemical conditions can be depicted and expectant paragenetic phases can be predicted in any deposits.

Keywords Activity diagrams · Common borates · Geochemical conditions · Diagenetic trend · Stability fields · Paragenetic relations

Introduction

There are over 230 borates are in the upper crust occurring in igneous, sedimentary, and metamorphic environments. Among borates, few of them occur in large quantities and some of them are very rare and only present in a few particular locations. Borate minerals, which are extensively used in industry, are found in great amounts in the deposits of Turkey, South America, and United States of America. All of these deposits are found in tectonically active extensional terrains and associated with continental sediments and volcanic soil of Neogene. However, only a small number of Ca-, Na-, Mg-, CaNa-, and CaMg-borates are common geologically and commercially, such as colemanite, borax, kernite, ulexite, probertite, and boracite. Some of the borates are found in the compositional series, such as inyoite, meyerhofferite, and colemanite; borax, tincalconite, and kernite; probertite and ulexite; suanite and ascharite; gowerite and nobleite; inderite and kurnakovite; somehow only one or two of them are found as preferred phases in most of the deposits. There have been many studies on their crystal structures (Christ and Clark 1977; Hawthorne et al. 2002) textural and mineralogical relations (Foshag 1921; Kistler and Helvacı 1994; Garsia-Veigas et al. 2011), geological settings (Helvacı and Firman 1976; Alonso et al. 1991; Helvacı and Alaca 1991) and their formation sequences and transformation mechanisms.

R. Birsoy (✉) · Ü. Özbaş
Department of Geological Engineering,
Faculty of Engineering, Dokuz Eylül University
Tınaztepe Campus, 35160 Buca, Izmir, Turkey
e-mail: rezan.birsoy@deu.edu.tr

Some of the borate minerals are precipitated from solution such as ulexite (Alonso 1986) and the others are products of diagenesis and post diagenetic reactions. According to experimental, textural, and structural data, colemanite were said to be formed as primary (Kistler and Helvacı 1994) or secondary phase (Christ and Garrels 1959). According to textural and structural data of borates in Kırka Deposit of Turkey, inyoite and ulexite were transformed to colemanite. Borax transforms to tincalconite, and ulexite replaces borax (İnan et al. 1973). Ulexite and colemanite appear to be primary (Helvacı 1977) in Emet deposit of Turkey.

All borates structurally contain combinations of $B(OH)_3$ and $B(OH)_4^-$ in their structures. Also thermodynamic concentrations (activity) of H^+, $B(OH)_3$, Na^+/H^+, $Ca^{2+}/(H^+)^2$, $Mg^{2+}/(H^+)^2$, CO_3^{2-}, HCO_3^- and H_2O are determining variables of the formation of borates (Christ et al. 1967). The study (Birsoy 1990) emphasizing on polymerization of borates demonstrates the effects of the activity of major cations (Ca, Na, and Mg), $B(OH)_4^-$, and pH on the paragenetic relations of polymers. Nevertheless, extent and limits of these variables have not been quantified. Consequently, the present study for various chemical environments has been undertaken to define the stability limits of common and rare borate occurrences through thermochemical calculations. Such work would provide valuable information about the formation and transformation conditions, and paragenetic relations for borate phases. Such work is also useful to explain some problematic field observations and/or to support the given explanations. For this purpose, borate minerals of Turkey, South America and United States, and minor extend of China and Kazakhstan are considered, and those deposits are evaluated by activity diagrams (Table 1).

Method of study

Thermodynamic data

Thermodynamic data for some borate minerals have been tabulated by Anovitz and Hemingway (2002) and Wagnam et al. (1982). However, thermodynamic data for some of the borates are not available. In such cases, empirical and theoretical approaches must be used to predict the thermodynamic properties of hydrated borates. Various methods are available to model the borate minerals (Mattigod 1983; Li et al. 2000). In the present study, free energy of formation ($\Delta G^0_{f,298}$) values for some borate minerals and ionic species were obtained from Anovitz and Hemingway (2002) and Helgeson et al. (1978) respectively. Free energy of formation of some borates has not been found in literature. To provide internal consistency in thermodynamic data, all other borates were recalculated applying both methods of Mattigod (1983) and Li et al. (2000). Mattigod's method provided the closest results to the experimental $\Delta G^0_{f,298}$ values. So Mattigod's (1983) structural empirical method was used to calculate $\Delta G^0_{f,298}$ values of borates. This method involves each of the borate minerals as a reaction of the type:

$$xB(OH)^-_{4(aq)} + aM^{v+}_{(aq)} + jH^+_{(aq)} + mH_2O_{(liq)} = M_a\left[B_xO_y(OH)_z\right]\cdot nH_2O_{(Solid)}$$

where x, y, z, a, and n are the stoichiometric coefficients of boron, oxygen, hydroxyl, cation and structural water in the borate polyanion in the solid, respectively. Major contribution of free energy changes (ΔG^0_r) in the above reaction come mainly from the free energy of polymerization of $B(OH)_4^-$ ions. In other words, the magnitude of ΔG^0_r would reflect the polymerization of borate minerals. The degree of polymerization value is expressed as an empirical relationship:

$$\Delta G^0_{r,298} = 124.26 - 82.37x + 2.95x^2$$

where x is the number of boron atoms in the polyanion unit. Then, applying this equation to the dehydration reaction of borate mineral given above results in;

$$\begin{aligned}\Delta G^0_{f,298}(\text{borate mineral}) &= \Delta G^0_{r,298} + x\Delta G^0_{f,298}B(OH)^-_{4(aq)} + a\Delta G^0_{f,298}M^{v+}_{(aq)} \\ &\quad + m\Delta G^0_{f,298}H_2O_{(liq)} + j\Delta G^0_{f,298}H^+\end{aligned}$$

With reference to the above equation, calculation of free energy of aksaite is;

$$6B(OH)_4^- + Mg^{++} + 4H^+ = MgB_6O_7(OH)_6\cdot 2H_2O + 9H_2O$$

$$\begin{aligned}\Delta G^0_{r,298} &= 124.26 - 82.37(6) + 2.95(36) \\ &= \Delta G^0_{f,298}\,\text{Aksaite} + 9\Delta G^0_{f,298}H_2O \\ &\quad - 6\Delta G^0_{f,298}B(OH)_4^- - \Delta G^0_{f,298}\,Mg^{++} - 2\Delta G^0_{f,298}\,H^+\end{aligned}$$

$$\begin{aligned}\Delta G^0_{f,298}\,\text{Aksaite} &= -263.76 - 9\Delta G^0_{f,298}H_2O \\ &\quad + 6\Delta G^0_{f,298}B(OH)_4^- + \Delta G^0_{f,298}Mg^{++} \\ &\quad + 2\Delta G^0_{f,298}H^+\end{aligned}$$

$$\begin{aligned}\Delta G^0_{f,298}\,\text{Aksaite} &= -263.76 - 9(-237.13) + 6(-1153.17) \\ &\quad + (-454.8) + 2(0) \\ &= -5{,}503.4\ \text{kj/mol}\end{aligned}$$

Stability limits of calcite, dolomite, and magnesite, which contribute as a source of cations and accompany to the occurrence of borates, are also considered. Free energies of all the phases used in the present study are given in Table 2.

Table 1 Mineral assemblages of major borate deposits

Deposits	Types of deposits	Associated minerals (in decreasing amounts)
Turkey		
Kırka[a]	Playa surface	Borax, ulexite, colemanite (hydroboracite, inderite, inyoite, kurnakovite, meyerhofferite, kernite, calcite, dolomite, smectite, illite, erionite)
Emet[b]	Permanent playa, lacustrine	Colemanite, probertite, ulexite, hydroboracite, meyerhofferite, dolomite, realgar, orpiment, montmorillonite
Bigadiç[c]	Playa setting	Colemanite, ulexite, probertite, hydroboracite, montmorillonite, opal-CT
Kestelek[d]	Shallow lake	Colemanite, ulexite, hydroboracite, smectite, illite, dolomite, quartz, clinoptilolite
Sultançayırı[e]	Playa lake	Pandermite (priceite), howlite, colemanite, clinoptilolite, illite, calcite, opal-CT
Italy		
Lardarello[f]	Volcanic lagoon	Sassolite, ammonium and magnesium sulfate
United States		
Kramer (Boron, CA)[g]	Shallow-permanent lake	Borax, kernite, ulexite, colemanite (probertite, hydroboracite, howlite, sassolite, inyoite meyerhofferite, tunnelite, realgar, and natrolite)
Searles Lake CA[h]	Playa lake	Borax (trona, halite, hanksite, searlesite and gaylusite)
Death Valley CA[i]	Playa setting	Colemanite, ulexite–probertite, hydroboracite, gypsum, halite, clinoptilolite, chabazite, phillipsite and calcite
South America		
Argentina		
Loma Blanca[j]	Lacustrine	Borax, ulexite, inyoite (colemanite, kernite, teruggite, realgar, orpiment, calcite, aragonite montmorillonite illite)
Tincalayu[j]	Lacustrine	Borax, kernite (ulexite, inyoite, kurnakovite, ezcurrite, ameghinite, inderite)
Sijes[j]	Lacustrine	Colemanite, inyoite, hydroboracite, ulexite, inderite, nobleite, gowerite, probertite
Chile		
Salar de Atacama[k]	Playa lake	Ulexite, halite (colemanite, ginorite)
Peru		
Laguna Salinas[l]	Playa lake	Ulexite, inyoite
Kazakstan[m]	Marine	Hydroboracite, ascharite, pandermite, colemanite, inyoite, ulexite, inderite
China		
Liaoning[n]	Silicate buried deposite	Ascharite, suanite, magnesite, magnetite
Quinghai[n]	Playa lake	Ulexite, pinnoite, hydroboracite, borax
Tibet		
Dujiali[n]	Lake; carbonate	Borax, tincalconite
Zhacang-caka[n]	Sulfate	Kurnakovite, pinnoite, inderite, ulexite
Nieer-Co[n]	Sulfate	Ulexite, kurnakovite
Da-Qaidam[n]	Sulfate	Pinnoite, ulexite, inderite

[a] Meixner (1965), Inan et al. (1973), Helvacı et al. (1993), Kistler and Helvac (1994), Palmer and Helvacı (1995), and Helvacı and Orti (1998)

[b] Helvacı and Firman (1976), Kistler and Helvacı (1994), and Helvacı and Orti (1998)

[c] Özpeker and İnan (1978), Helvacı and Alaca (1991), Kistler and Helvacı (1994), and Helvacı and Orti (1998)

[d] Kistler and Helvacı (1994), Helvacı (1994), and Helvacı and Orti (1998)

[e] Meixner (1965), and Kistler and Helvacı (1994), Orti et al. (1998), and Helvacı and Orti (1998)

[f] Kistler and Smith (1983)

[g] Siefke (1991), Kistler and Helvacı (1994), and Bernard and Kistler (1966)

[h] Smith (1979)

[i] Allen and Kramer (1957), Barker and Barker (1985), Evans et al. (1976), Barker and Wilson (1976), Chandler (1996), Countryman (1977), Wendel (1978), and Castor (1993)

[j] Alonso (1986) and Alonso and Gonzales-Barry (1995)

[k] Garrett (1998), Alonso et al. (1991), and Kistler and Helvacı (1994)

[l] Kistler and Helvacı (1994) and Garrett (1998)

[m] Garrett (1998) and Kistler and Helvacı (1994)

[n] Garrett (1998) and Smith and Medrano (2002)

Table 2 Free energies of formation, structural subdivisions and divisions of borates

Mineral	Chemical formula	Free energy ($\Delta G^0_{f,\ 298}$ kJ/mol)	Structural subdivisions and divisions[e]	Fundamental building block (FBB)[e]
Ca-Borates				
Inyoite	$Ca_2B_6O_6(OH)_{10}\cdot 8H_2O$	−8,218.78[a]	Neso-triborate	3(Δ + 2T)
Meyerhofferite	$Ca_2B_6O_6(OH)_6\cdot 2H_2O$	−6,803.00[c]	Neso-triborate	3(Δ + 2T)
Colemanite	$Ca_2B_6O_8(OH)_6\cdot 2H_2O$	−6,334.60[a]	Ino-triborate	3(Δ + 2T)
Gowerite	$CaB_6O_8(OH)_4\cdot 3H_2O$	−5,602.00[b]	Phyllo-pentaborate	5(3Δ + 2T) + Δ
Nobleite	$CaB_6O_9(OH)_2\cdot 3H_2O$	−5,370.60[a]	Phyllo-hexaborate	6(3Δ + 3T)
Pandermite	$Ca_4B_{10}O_{19}\cdot 7H_2O$	−10,582.00[c]	Unclassified	6(2Δ + 4T)
Tertschite	$Ca_4\ [B_5O_7(OH)_5]_2\cdot 15H_2O$	−13,936.60[b]	Unclassified	Unclassified
Ginorite	$Ca_2B_{14}O_{20}(OH)_6\cdot 5H_2O$	−11,932.95[b]	Phyllo-hexaborate	6(3Δ + 3T) + 6(3Δ + 3T) +2Δ
Na-Borates				
Borax	$Na_2B_4O_5(OH)_4\cdot 8H_2O$	−5,516.00[a]	Neso-tetraborate	4(2Δ + 2T)
Tincalconite	$Na_2B_4O_5(OH)_4\cdot 3H_2O$	−4,323.50[a]	Neso-tetraborate	4(2Δ + 2T)
Kernite	$Na_2B_4O_6(OH)_2\cdot 3H_2O$	−4,084.50[a]	Ino-tetraborate	4(2Δ + 2T)
Mg-Borates				
Suanite	$Mg_2B_2O_5$	−2,445.00[c]	Neso-diborate	2(2Δ); 2(2Δ) + OH
Ascharite	$Mg_2B_2O_4(OH)_2$	−2,716.50[a]	Neso-diborate	2(2Δ); 2(2Δ) + OH
Pinnoite	$MgB_2O_4\cdot 3H_2O$	−2,596.00[a]	Neso-diborate	2(2T)
Inderite	$MgB_3O_3(OH)_5\cdot 5H_2O$	−4,248.20[a]	Neso-triborate	3(Δ + 2T)
Kurnakovite	$MgB_3O_3(OH)_5\cdot 5H_2O$	−4,366.90[a]	Neso-triborate	3(Δ + 2T)
Aksaite	$MgB_6O_7(OH)_6\cdot 2H_2O$	−5,503.40[b]	Neso-hexaborate	6(3Δ + 3T)
Borates,				
Sassolite	H_3BO_3	−969.40[a]	Isolated-monoborate	1(Δ)
Metaborite	HBO_2	−723.40[a]	Tecto-megaborate	∞(∞T)
Ca–Na-Borates				
Ulexite	$NaCaB_5O_6(OH)_6\cdot 5H_2O$	−6,044.30[a]	Neso-pentaborate	5(2Δ + 3T)
Probertite	$NaCaB_5O_7(OH)_4\cdot 3H_2O$	−5,373.08[b]	Ino-pentaborate	5(2Δ + 3T)
Ca–Mg-Borates				
Hydroboracite	$CaMg[B_3O_4]_2(OH)_6\cdot 3H_2O$	−6,474.20[a]	Ino-triborate	3(Δ + 2T)
Inderborite	$CaMg[B_3O_3(OH)_5]_2\ (H_2O)_4\cdot 2H_2O$	−7,646.70[a]	Ino-triborate	3(Δ + 2T)
Carbonates				
Magnesite	$MgCO_3$	−1,027.87[d]	–	
Dolomite	$CaMg(CO_3)_2$	−2,167.23[d]	–	
Calcite	$CaCO_3$	−1,130.10[d]	–	

[a] Experimental (Anovitz and Hemingway 2002)

[b] Estimated in present study (Mattigod 1983)

[c] Estimated (Anovitz and Hemingway 2002)

[d] Helgeson et al. (1978)

[e] Strunz (1997)

Construction of activity diagrams

The activity diagrams constructed here consist of a five-component system CaO–MgO–Na_2O–B_2O_3–H_2O + CO_2. This system can be represented with various functions, such as $\log[a_{Ca^{2+}}/(a_{H^+})^2]$, $\log[a_{Mg^{2+}}/(a_{H^+})^2]$, $\log[a_{Na^+}/(a_{H^+})^2]$, $\log[a_{Ca^{2+}}/(a_{Na^+}\times a_{H^+})]$, and $\log[a_{Ca^{2+}}/a_{Mg^{2+}}]$, versus $\log[a_{H_2O}]$ and $\log[a_{B(OH)_3}]$. As an example, the stability line between colemanite and nobleite in the $\log[a_{Ca^{2+}}/(a_{H^+})^2] - \log[a_{H_2O}]$ plane; by using hydrolysis reaction, $B(OH)_{3(aq)}$ was eliminated and the following equilibrium reaction was obtained.

$$\underset{\text{(Colemanite)}}{Ca_2B_6O_8(OH)_6\cdot 2H_2O} + 2H^+ = \underset{\text{(Nobleite)}}{CaB_6O_9(OH)_2\cdot 3H_2O} + Ca^{2+} + 2H_2O$$

$$\log K = 2\log[a_{H_2O}] + \log\left[a_{Ca^{2+}}/(a_{H^+})^2\right]$$

$$\log\left[a_{Ca^{2+}}/(a_{H^+})^2\right] = -2\log[a_{H_2O}] + \log K$$

The stability line between colomanite and nobleite in the $\log[a_{Ca^{2+}}/(a_{H^+})^2] - \log[a_{B(OH)_3}]$ plane was calculated as:

$$\log\left[a_{Ca^{2+}}/(a_{H^+})^2\right] = \log K - 2.$$

Similar types of equations were derived for all possible mineral pairs and using these line equations, a series of stability diagrams were constructed (Garrels and Christ 1965). As some mineral pairs occupy the same stability area, for example, gowerite–nobleite, ulexite–probertite, kurnakovite–inderite, and ascharite–suanite, they were plotted on different diagrams suppressing one of them or pair of them separately. Furthermore, triples of colemanite–meyerhofferite–inyoite and borax–tincalconite–kernite are just a function of the activity of the H_2O. As a consequence these mineral pairs were evaluated only in the plane of activity of metal versus activity of the H_2O.

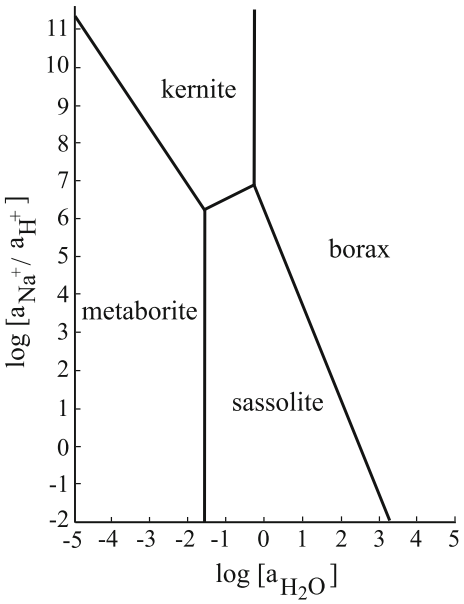


Fig. 1 Activity diagram for the system Na-B–H_2O balanced with respect to B at 25°C. No stability field for tincalconite, but forms on the kernite–borax stability line as metastable phase

Results

A series of diagrams for five-component systems are shown in Figs. 1, 2, 3, 4, 5, 6, 7, 8 and 9. Figures 1, 2, 3, 4, 5 are activity diagrams plotted on the $\log[a_{Mb^{n+}}/(a_{H^+})^n]$ and $\log[a_{Mb^{n+}}/a_{Mc^{(n-1)+}}(a_{H^+})]$ versus $\log[a_{H_2O}]$ plane where b: Na, Ca and Mg, and c: Na and Mg. Figures 6, 7, 8, 9 are activity diagrams plotted on the $\log[a_{Mb^{n+}}/(a_{H^+})^n]$ and $\log[a_{Mb^{n+}}/a_{Mc^{(n-1)+}}(a_{H^+})]$ versus $\log[a_{B(OH)_3}]$ plane. In the diagrams (Figs. 1, 2, 3, 4, and 5), along horizontal axis, decreasing activity of water have same qualitative effect of increasing evaporation rate, dehydration rate, temperature and depth of burial (Christ et al. 1967). However, increasing activity of boron (Figs. 6, 7, 8 and 9) depends on addition of boron, and/or increasing burial depth, and/or evaporation trend. In all diagrams, along the vertical axis, pH and concentrations of cations and ratios of cations increase.

Diagrams on $\log[a_{Mb^{n+}}/(a_{H^+})^n]$ and $\log[a_{Mb^{n+}}/(a_{Mc}^{(n-1)+})(a_{H^+})]$ versus $\log[a_{H_2O}]$ plane.

Figures 1, 2, 3, 4, and 5 provide activity diagrams constructed to evaluate the stability fields of single and double metal borates in relation with evaporation and/or diagenetic trend.

Figure 1 illustrates Na_2O–B_2O_3–H_2O system with three Na-borates (borax, tincalconite, and kernite) plus sassolite and metaborite. Kernite and borax are stable phases. But tincalconite does not form its stability area, because kernite–tincalconite and tincalconite–borax stability lines coincide with the kernite–borax line. Consequently it forms as metastable phase. Borax is the primary phase, but depending on the slope of evaporation or digenetic trend, can transform to tincalconite–kernite or sassolite–metaborite. Associations of borax–kernite–sassolite and sassolite–metaborite–kernite would depend on the pH besides decrease in $\log[a_{H_2O}]$ due to increase in concentration of the solution upon evaporation of water or, influx of the more concentrated solution or, increase in temperature or, burial of the system. Based on these changes, new phases will have lower water content, but cause more complex structures with higher degree of polymerization (Christ et al. 1967; Garrett 1998).

In CaO–B_2O_3–$H_2O \pm CO_2$ system, eight Ca-borates (inyoite, meyerhofferite, colemanite, gowerite, nobleite,

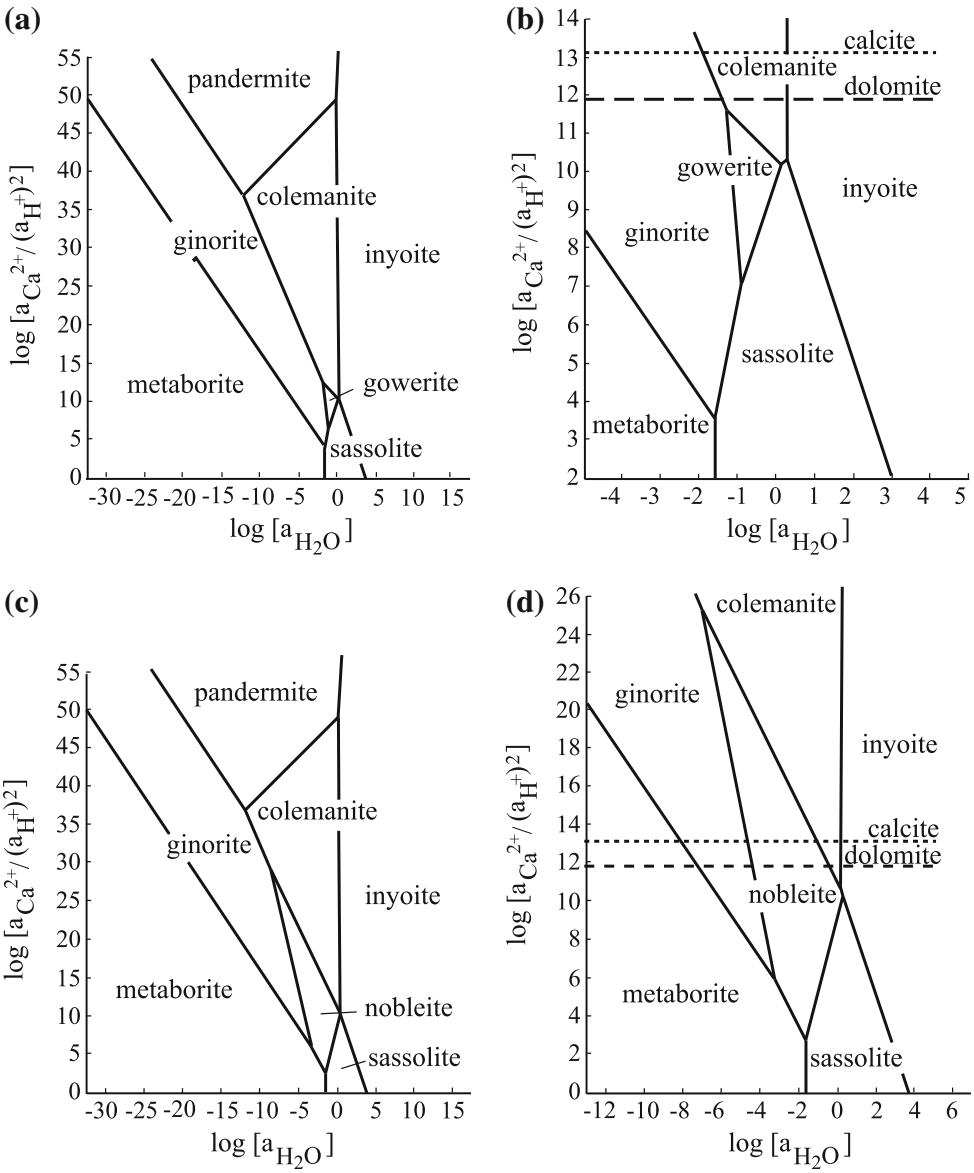


Fig. 2 Activity diagrams for the system Ca–B–H_2O plus CO_2 balanced with respect to B at 25°C. **a** Suppression of nobleite, **b** scale expansion of (**a**), **c** suppression of gowerite, and **d** expansion of (**c**). In all diagrams, stability line of meyerhofferite locates on the colemanite–inyoite stability line as metastable phase. Saturation lines for calcite and dolomite are indicated as *dashed lines*

pandermite, tertschite, and ginorite), and sassolite and metaborite are considered. Activity diagrams (Fig. 2a–d) are quite similar to the schematic diagrams of Christ et al. (1967), except the gowerite stability field is included in the nobleite stability field at the present study. For this reason, Fig. 2a, b is constructed by suppressing the nobleite and Fig. 2c, d, the gowerite. Nobleite has wider stability field than gowerite, indicating that occurrence of nobleite has higher possibility than gowerite. At given thermochemical conditions (Fig 2a–d), colemanite–meyerhofferite and meyerhofferite–inyoite stability lines coincide with colemanite–inyoite stability line, indicating the metastability of meyerhofferite. Meyerhofferite can form on the inyoite–colemanite stability line. But tertschite appears in an unstable phase. If they are present in any deposits, they possibly persist as metastable phases. The complexity and the polymerization degree of phases have positive trends with dehydration, pH and depth of burial (Schindler and Hawthorne 2001). Triple points on Fig. 2a, b (inyoite–colemanite–sassolite, gowerite–colemanite–ginorite, inyoite–colemanite–pandermite, and ginorite–colemanite–pandermite) indicate the increasing degree of evaporation and diagenetic processes, and also thermochemical properties of the deposits. On the other hand, Fig. 2c, d shows that nobleite persists to change to the more complex phases with increasing evaporation and diagenetic processes.

Six Mg-borates (suanite, ascharite, pinnoite, inderite, kurnakovite, and aksaite) plus sassolite and metaborite are plotted in Fig. 3a, b in the system of MgO–B_2O_3–H_2O ± CO_2. Inderite and kurnakovite are polymorph phases and they appear as primary phases in such systems. When kurnakovite is suppressed (Fig. 3a), suanite, ascharite,

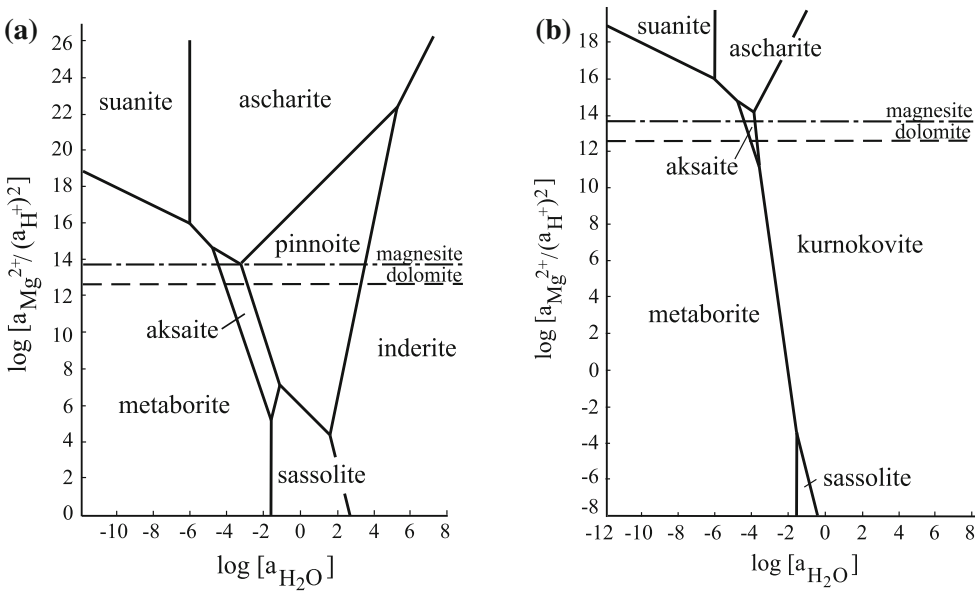


Fig. 3 Activity diagrams for the system Mg–B–H_2O balanced with respect to B at 25°C. **a** Suppression of kurnakovite, **b** suppression of inderite. Saturation lines for dolomite and magnesite are indicated as *dashed lines*

pinnoite, inderite, aksaite, metaborite, and sassolite become stable phases. On the contrary, suppressing inderite (Fig. 3b) results in disappearance of the stability field of pinnoite and there is also a decrease in the stability fields of aksaite, ascharite, and sassolite. As seen from the diagrams, kurnakovite–ascharite–aksaite and ascharite–inderite–pinnoite associations are favored in higher pH values.

First of the double-cation-bearing borates considered is the system of CaO–Na_2O–B_2O_3–H_2O. Thirteen phases are calculated for plotting Fig. 4a–b. Seven (kernite, probertite, ulexite, borax, inyoite, colemanite, and pandermite) out of the 13 borates are plotted as stable phases. In the double-cation-bearing system, only inyoite, colemanite, and pandermite appear as stable phases for Ca-borates. Meyerhofferite forms on the inyoite–colemanite stability line. Probertite has larger stability field and includes the stability field of ulexite. Calculated ulexite–colemanite, ulexite–inyoite and ulexite–borax stability lines resulted in very small stability field of ulexite (Fig. 4b–c). In some recent lake occurrences, ulexite is found as primary phase (Salinas at South America). In these deposits, ulexite forms before probertite, indicating the rate of evaporation or kinetically high rate of ulexite crystallization (Garrett 1998) or these lakes have exactly at the thermochemical condition of ulexite formation (Fig. 4c). This diagram clarifies and also provides guidance to the textural relations of borate assemblages of Kırka (İnan et al. 1973) and Emet (Helvacı 1977) deposit of Turkey.

Second of the double-cation-bearing borate is the system of CaO–MgO–B_2O_3–H_2O. Sixteen phases are calculated for plotting (Fig. 5a, b). Four borate phases; colemanite, inyoite, hydroboracite, and inderite are stable, and meyerhofferite is metastable in this system (Fig. 5a). In such system, uncommon phases, gowerite, nobleite, ginorite, suanite, ascharite–pinnoite, and aksaite do not appear as stable phases. As inderite and kurnakovite are polymorph phases, when inderite is suppressed, stable phases are kurnakovite, hydroboracite, colemanite, and inyoite (Fig. 5b). The stability field of inyoite moves to a higher activity ratio of $\log[a_{Ca^{2+}}/a_{Mg^{2+}}]$ and decreases its stability area (Fig. 5b). All stable phases are triborates and with decreasing $\log[a_{H_2O}]$ and increasing $\log[a_{Ca^{2+}}/a_{Mg^{2+}}]$, transform from neso- to ino-borates corresponding to diagenetic trend.

Diagrams on $\log[a_{Mb^{n+}}/(a_{H^+})^n]$ and $\log[a_{Mb^{n+}}/(a_{Mc}^{(n-1)+})(a_{H^+})]$ versus $\log[a_{B(OH)_3}]$ plane

All diagrams in this section are plotted assigning the value of the a_{H_2O} equal to unity.

Since all Na-borates are tetraborates and a function of H_2O, they cannot be represented on $\log[a_{Mb^{n+}}/(a_{H^+})^n]$ versus $\log[a_{B(OH)_3}]$ plane. Therefore $\log[a_{Na^+}/a_{H^+}]$ versus $\log[a_{B(OH)_3}]$ diagram cannot be plotted.

Plotting of $\log[a_{Ca^{2+}}/(a_{H^+})^2]$ versus $\log[a_{B(OH)_3}]$ diagram resulted in five stable phases out of ten total phases (Fig. 6a–b). However, the stability fields of inyoite and meyerhofferite are included in the stability field of colemanite. As gowerite and nobleite occupy the same stability field, both suppressions are shown on Fig. 6a, b, respectively. Gowerite occupies a smaller stability field than nobleite. Sassolite is unstable even though it was stable in the $\log[a_{Ca^{2+}}/(a_{H^+})^2] - \log[a_{H_2O}]$ diagrams. Furthermore, an increasing polymerization degree and increasing

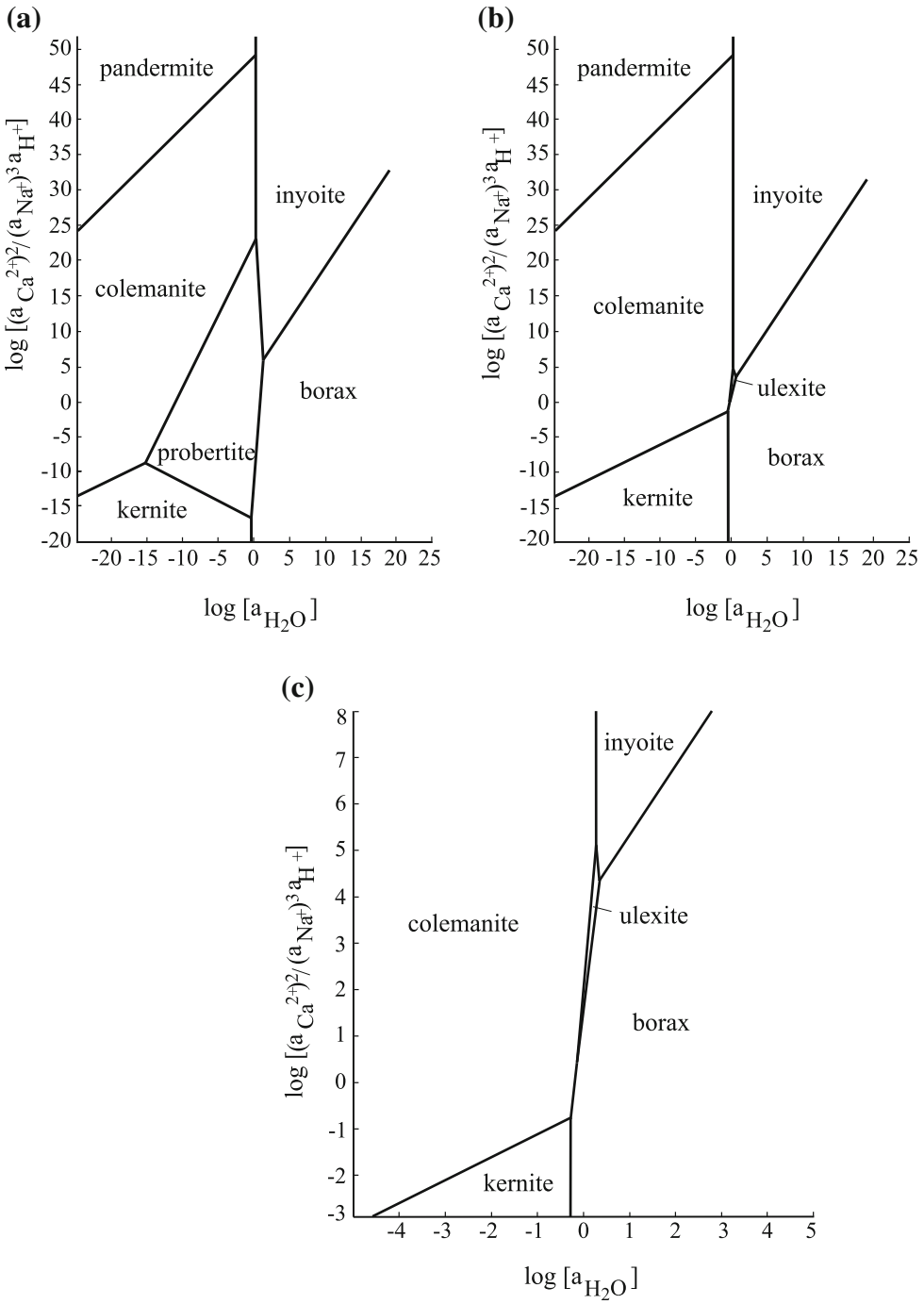


Fig. 4 Activity diagrams for the system Ca–Na–B–H_2O balanced with respect to B at 25°C. **a** Suppression of ulexite, **b** suppression of probertite, **c** scale expansion of (**b**)

activities of Ca and $B(OH)_3$ ions and pH show a positive correlation trend.

When the phases of $\log[a_{Mg^{2+}}/(a_{H^+})^2] - \log[a_{B(OH)_3}]$ plotting plane considered, couples those of suanite–ascharite and kurnakovite–inderite could not be plotted on the same plotting plane. Therefore, four couple suppressions were made to construct the activity diagrams (Fig. 7a–d). Inderite is always an unstable phase in the related diagrams (Fig. 7a, d). In all four diagrams, increasing polymerization degree and increasing activities of Mg and B have positive correlation trend. Thermodynamically, kurnakovite is the most common Mg-borate mineral.

Figure 8a–f shows the series of diagrams in which six couple phases were suppressed, namely, tincalconite–kernite–ulexite, tincalconite–kernite–probertite, borax–kernite–ulexite, borax–kernite–probertite, tincalconite–borax–ulexite, and tincalconite–borax–probertite. Because of larger stability field occupation of probertite than ulexite, ulexite is

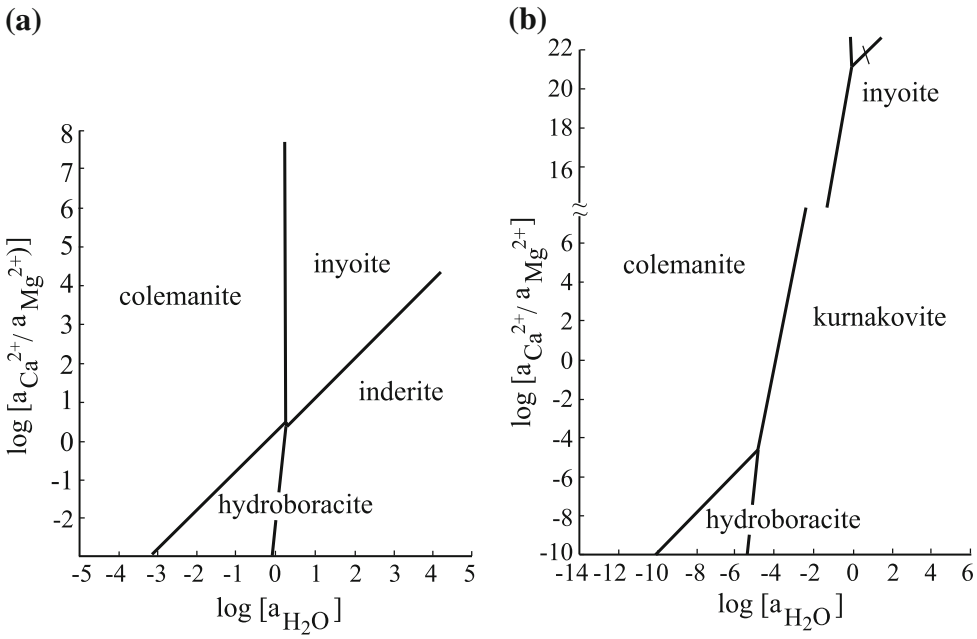


Fig. 5 Activity diagrams for the system Ca–Mg–B–H_2O balanced with respect to B at 25°C. **a** Suppression of kurnakovite, **b** suppression of inderite. In both diagrams, stability line of meyerhofferite locates on the colemanite–inyoite stability line as metastable phase

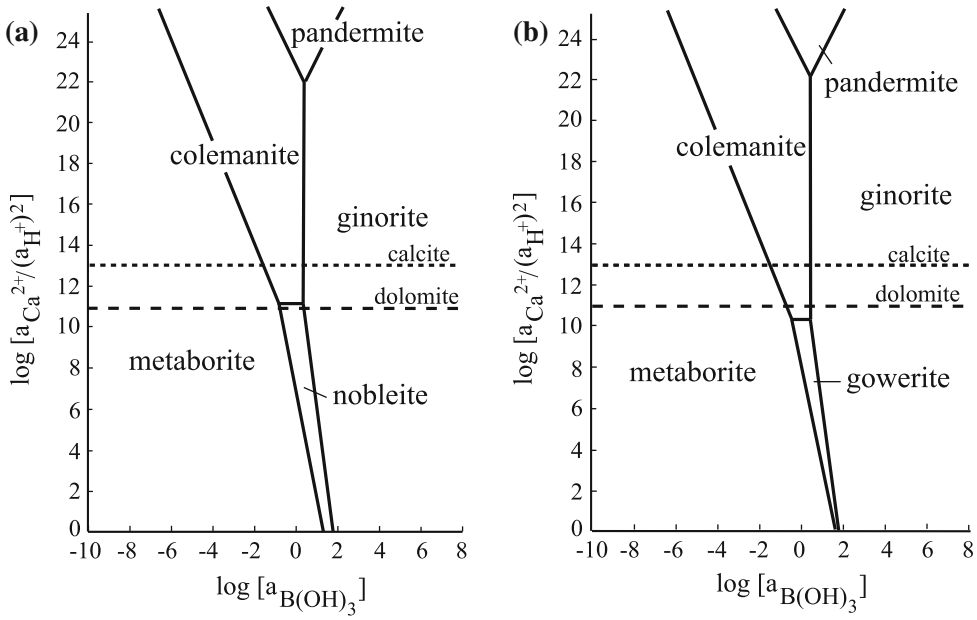


Fig. 6 Activity diagrams for the system Ca–B–H_2O plus CO_2. Activity of H_2O is assigned to unity. **a** Suppression for gowerite, **b** suppression for nobleite. Stability fields of meyerhofferite and inyoite are included in the stability field of colemanite. Saturation lines for calcite and dolomite are indicated as *dashed lines*

included in the stability field of probertite. Ulexite appears on the diagram when probertite is suppressed. Nobleite, gowerite, inyoite are unstable phases on this type of diagrams. Increasing Ca/Na activity plus pH and $B(OH)_3$ activity show increasing trend with the structural complexity and the polymerization degree of the borates.

Associations of Mg-, Ca- and CaMg-borates are not so common. However, their deposits can be found in various parts of the world. Inderite and kurnakovite are polymorph borates and both are not stable in this system. Indicating that, in the systems which contains two or more cations, kurnakovite and inderite are not stable phases. Ascharite–suanite and hydroboracite–inderborite are a function of activity of the H_2O, i.e., not independent variables. Four suppressions consist of ascharite–hydroboracite, ascharite–inderborite, suanite–hydroboracite, and suanite–inderborite were considered in Fig. 9a–d, respectively. Four borates are stable and hydroboracite has a larger stability field than

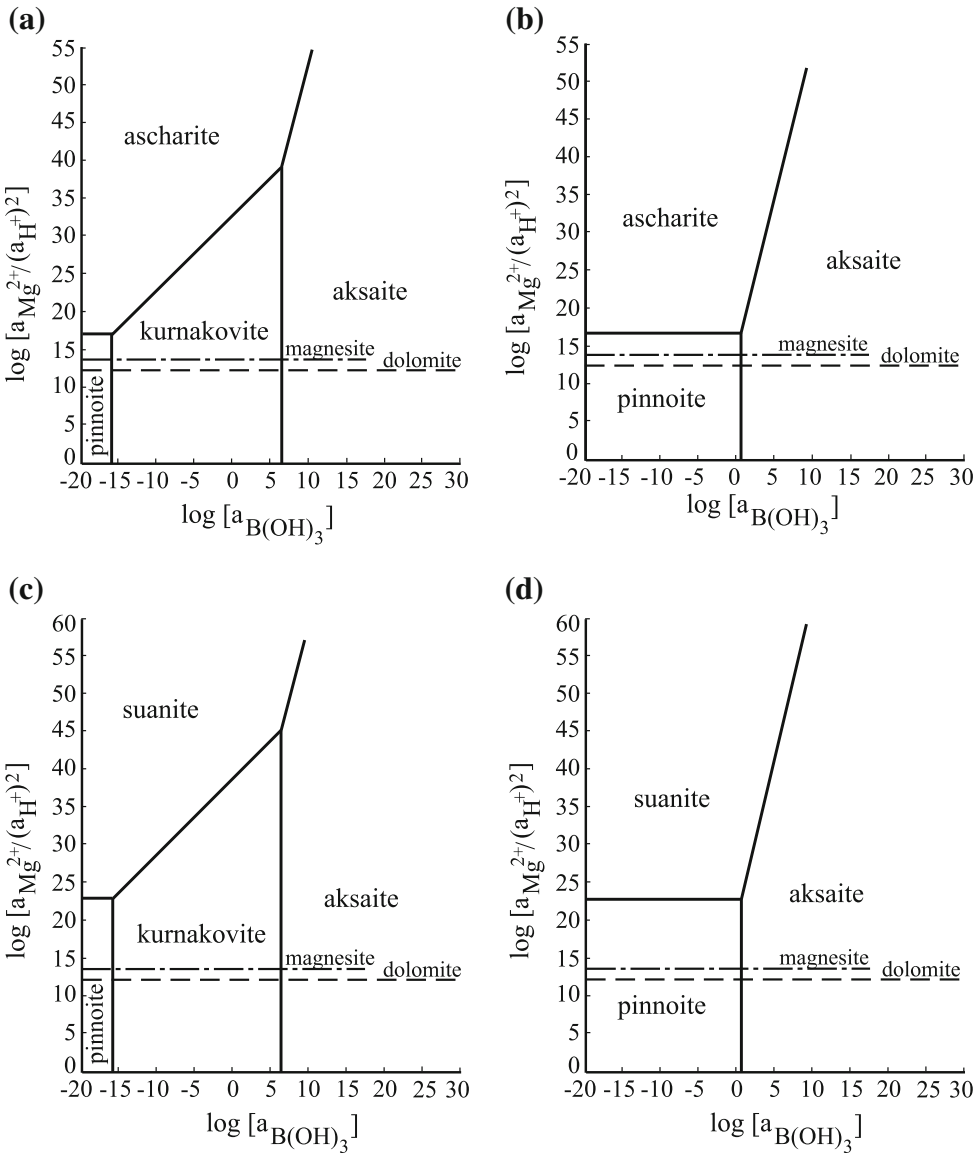


Fig. 7 Activity diagrams for the system Mg–B–H_2O. Activity of H_2O is assigned to unity. **a** Suppression for suanite and inderite, **b** suppression for suanite and kurnakovite, **c** suppression for ascharite and inderite, **d** suppression for ascharite and kurnakovite. Saturation lines for dolomite and magnesite are indicated as *dashed lines*

inderborite indicating the reason of its abundance. Ascharite and hydroboracite are both more favorable than suanite and inderborite respectively.

Discussion

Activity–activity diagrams of borates at isobaric and isothermal conditions provide information about the trend of crystallization sequences and diagenetic relations with respect to the chemical activities of metals, H_2O and $B(OH)_3$, and pH. Similar but schematic diagrams were constructed by Christ et al. (1967). In the present study, all variables, and stable, metastable, and unstable phases are considered in real numbers and the conditions for common deposits are demonstrated. Direction of $\log[a_{Mb^{n+}}/(a_{H^+})^n]$ and $\log[a_{Mb^{n+}}/(a_{Mc^{(n-1)+}})(a_{H^+})]$ versus $\log[a_{H_2O}]$ axes on the diagram indicate that as $\log[a_{Mb^{n+}}/(a_{H^+})^n]$ or $\log[a_{Mb^{n+}}/(a_{Mc^{(n-1)+}})(a_{H^+})]$ increases and $\log[a_{H_2O}]$ decreases, pH, degree of evaporation, depth of burial and/or temperature increase. Likewise, increasing direction of $\log[a_{Mb^{n+}}/(a_{H^+})^n]$ or $\log[a_{Mb^{n+}}/(a_{Mc^{(n-1)+}})(a_{H^+})]$ and $\log[a_{B(OH)_3}]$ axes shows the increasing trend of temperature, depth of burial and/or degree of evaporation. These trends are sort of indication of crystallization and transformation sequences. Any deposit can be interpreted over these activity diagrams. In other words, formation parameters and sequences, and forthcoming transformations can be described. Phases, which are considered during the construction of diagrams but do not appear on the diagrams, can be unstable or metastable phases and may persist in deposits depending on the changing the value of variables, such as

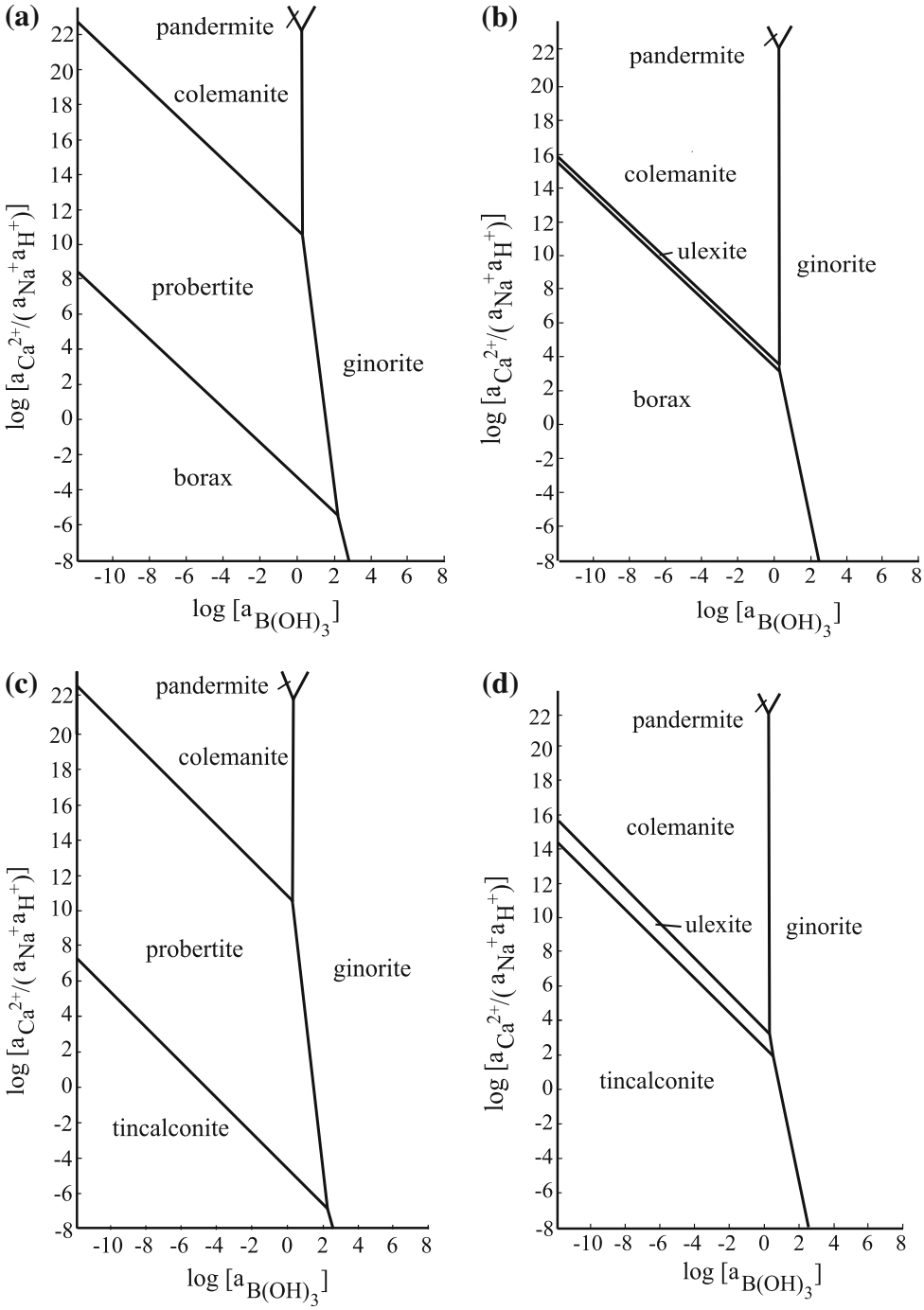
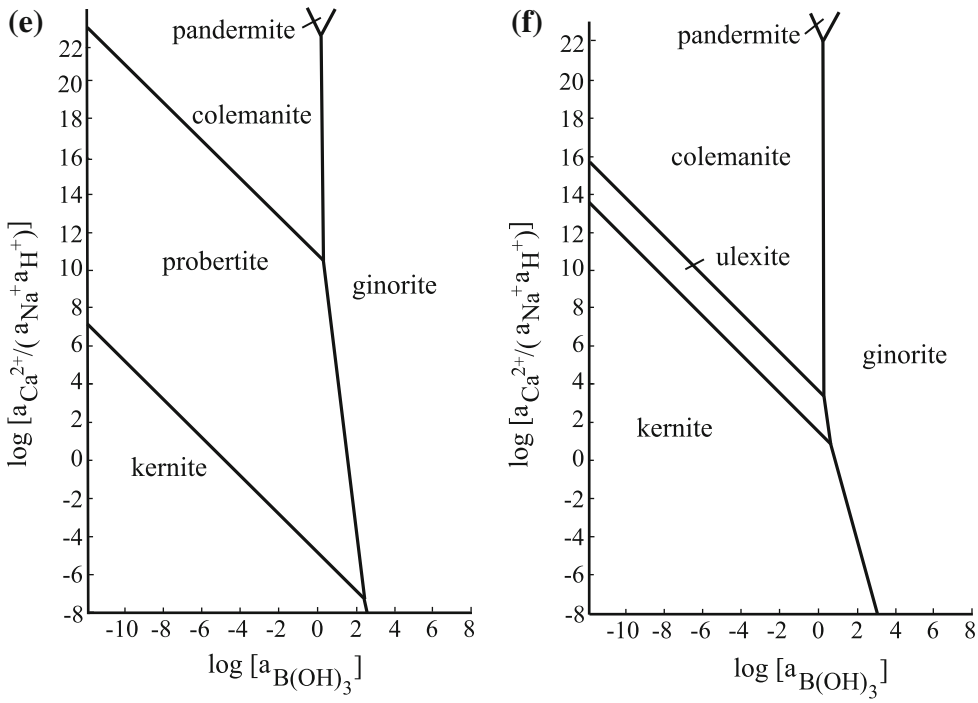


Fig. 8 Activity diagrams for the system Ca–Na–B–H_2O. Activity of H_2O is assigned to unity. **a** Suppression for tincalconite-kernite-ulexite, **b** suppression for tincalconite–kernite–probertite, **c** suppression for borax–kernite–ulexite, **d** suppression for borax–kernite–probertite, **e** suppression for tincalconite–borax–ulexite, and **f** suppression for tincalconite–borax–probertite

crystallization rate, evaporation rate, and/or changing composition of the solution. Furthermore, according to Schindler and Hawthorne (2001), degree of structural units (degree of polymerization) increases with decreasing activity of H_2O and proportion of the $^{[4]}B$ (Schindler and Hawthorne 2001) in the structural unit increases with increasing pH (Hawthorne et al. 2002). These relations are consistent with the constructed diagrams.

Kırka (Turkey) is the world's largest borax deposit. Minor amounts of ulexite, colemanite, hydroboracite, inderite, inyoite, kurnakovite, and tincalconite are also present. Borax is the first phase crystallized from solution when the solution is Na rich (Figs. 1, 4a–c, and 8a, b). Next to be formed phase is ulexite even though probertite has a larger stability area than ulexite (Figs. 4b, c, 8b, d). This is because of probertite (ino-pentaborate) being structurally more complex than ulexite (neso-pentaborate). Progressing evaporation and increasing burial depth, the other minor phases such as inderite, hydroboracite, inyoite, and kurnakovite form in the pore solutions which are locally

Fig. 8 continued



concentrated in Mg, and Ca (Fig. 5a, b). In any carbonate containing salt brine borax, kernite (Fig. 1), and then ulexite and colemanite (Figs. 4b, c, and 8b, d, f) form with increasing evaporation rate or temperature and depth of burial. This result agrees with the observed setting and sequence of Kırka deposit (İnan et al. 1973) and model for evaporation of lake.

Borax deposit of Kramer (Boron, CA) and Searles Lake (CA) are indicated in Figs. 1, 4a–c and 8b. Figure 1 shows how the structural properties and dehydration, increasing temperature or evaporation relation worked together for the assemblages of these phases. Formation sequences from borax to kernite (Fig. 1), borax to probertite (Figs. 4a and 8a), borax to inyoite (Fig. 4a–c) and sassolite to kurnakovite–inyoite (Fig. 2a–d) in Kramer borax deposit are also described with decreasing water activity, increasing cation/cation ratio and pH. These diagrams represent the relation between the phases in ideal evaporation processes. The phases which do not appear on the diagrams, but are found in the deposit can be formed by diagenetic activities such as dissolution and/or recrystallization (Bernard and Kistler 1996). Similar interpretations can be made for world's other borax deposits. For example, for the borax deposits of Loma Blanca (Figs. 4b, c and 8b, f) and Tincalayu (Figs. 1, 4b, c, 5b, 8b, f) of Argentina, thermochemical conditions for borax–kernite (Fig. 1, 4a–c), borax–ulexite–colemanite (Fig. 4b, c, 8b), ulexite–colemanite–kernite (Fig. 8f) and inyoite–kurnakovite (Fig. 5b) associations are clearly represented. Ginorite is not found in any of these deposits. The most likely activity of $B(OH)_3$ never reaches the certain required value for ginorite formation of any diagenetic process. Dujiali (Tibet) borax deposits can be represented by Fig. 1. Tincalconite is metastable phase with respect to borax, and tincalconite persists throughout the deposit. This is the most probable case for this type of deposits.

Colemanite deposits are considered in two different types of occurrences, one with Na-borates and the other with Mg-borates. Colemanite is the major mineral in Emet, Bigadiç and Kestelek of Turkey, and Death Valley of United States (Figs. 2a–d, 4a–c, 5a, b and 6a, b). However, large amount of probertite at the lower part of Emet deposit and minor amounts of ulexite occur at the upper zones of the deposit (Garsia-Veigas et al. 2011). For all these deposits, occurrences are represented by Figs. 4a–c and 8b, d and f. According to the activity–activity diagrams, the primary phase from the solution is never colemanite, except initial solution composition is in the colemanite stability area. In lower concentrated solutions, minerals such as inyoite initially form, then, due to dehydration with increasing pH and cation activity/or increasing $\log[a_{B(OH)_3}]$, colemanite and other complex borates can form in such deposits. Ulexite forms as stable phase in the system. Besides ulexite, Emet and Kestelek deposits contain hydroboracite, and Bigadiç and Death Valley, hydroboracite and probertite. During evaporation and later ongoing diagenetic changes, transformations to more complex phases can be interpreted by Figs. 5a, 8a, b, and 9b, d. The Colemanite deposit of Sijes (Argentina), besides hydroboracite and inyoite, has ulexite, inderite, nobleite, and gowerite. These associations and formation and/or

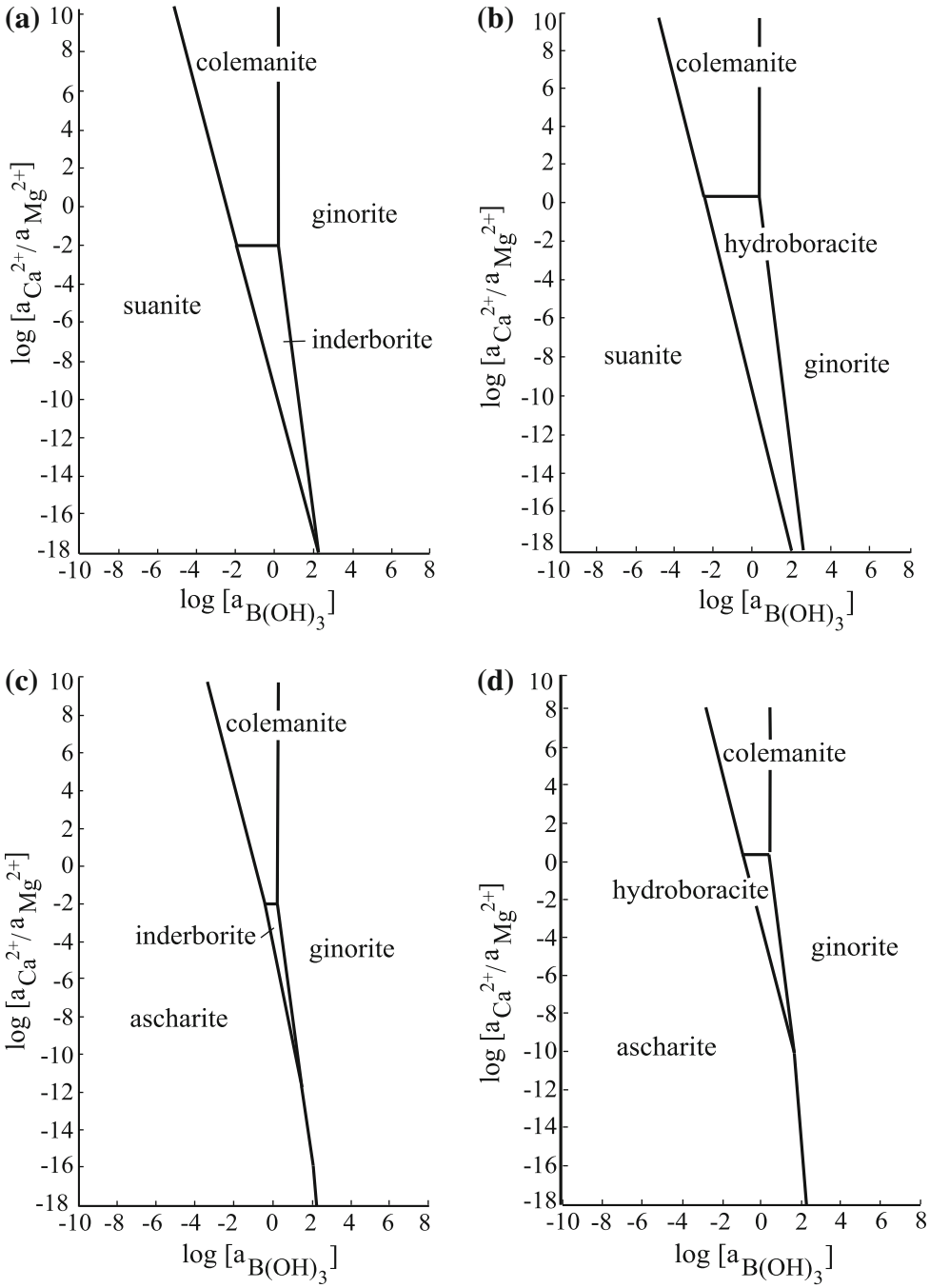


Fig. 9 Activity diagrams for the system Ca–Mg–B–H_2O. Activity of H_2O is assigned to unity. **a** Suppression for ascharite–hydroboracite, **b** suppression for ascharite–inderborite, **c** suppression for hydroboracite–suanite, and **d** suppression for suanite–inderborite. Stability fields of meyerhofferite and inyoite are included in the stability field of colemanite

transformation sequences are represented by Figs. 2a–d, 4b, c and 5a. Depending upon the initial activities of the cations, H^+ and $B(OH)_3$ of the depositing system, orders of inyoite–colemanite–nobleite–ginorite or inyoite–colemanite–gowerite are possible.

Pandermite (priceite) with colemanite occurrences is known to be found in Sultançayırı (Turkey). According to Figs. 2a–d and 4a, b, pandermite forms after colemanite or inyoite as a secondary phase during burial or late diagenesis. Figures 6a, b and 8a–f also indicate that pandermite forms after colemanite. These observations are also in agreement with the pandermite association of Death Valley, CA (Allen and Kramer 1957).

Ulexite is in the stability field of probertite and when probertite is suppressed ulexite has a very small stability field (Figs. 4a–c, 8a–f). However, in most of the lakes, ulexite is found as the primary phase. Ulexite (neso-pentaborate) is structurally less complex than probertite (ino-pentaborate) and kinetic factors also control the formation of ulexite. Figure 4b, c represents the ulexite–inyoite associations of Laguna Salinas (Peru). At these types of occurrences, composition of the solution is in a

very small stability area (Fig. 4b, c). At the other actual lakes such as Quinghai (China) and Nieer-Co (Tibet), ulexite is the main and first forming phase. Minor amounts of Mg-borates are also present. In fact, tincalconite can be formed as metastable phase in the borax stability field with kernite. At the evaporating condition, borax formations are followed by ulexite–probertite and colemanite phases. As ulexite thermodynamically has very small stability field, probertite forms as a natural consequence. However, ulexite is kinetically favorable than probertite at surface condition, ulexite forms instead of probertite as in the Emet deposit.

Mg- and MgCa-borates are also found in actual lakes of China and Tibet, and Marine deposit of Kazakhstan. Liaoning (China) is an example of a silicate buried lake. Ascharite and suanite of this deposit represented by Fig. 3a, b are formed after burial or late diagenesis. Borate association of Kazakhstan such as ascharite–inderite (Fig. 3a, b), inderite–hydroboracite–inyoite–colemanite (Fig. 5a) indicate very restricted stability field. Inderborite has smaller stability field than hydroboracite (Fig. 9a–d) and is also unstable (Fig. 5a). Kurnakovite, pinnoite, and inderite association of Zhacang-caka (Tibet) is represented by Figs. 3a, b and 7a, c. Kurnakovite forms as primary phase and also persists to the late stages of evaporation (Fig. 5a, b).

Conclusions

1. In this study, 23 borates are calculated for the activity diagrams. Among these diagrams tertschite and inderborite are unstable, tincalconite and meyerhofferite are metastable phases. Furthermore, ulexite has a smaller stability field than probertite and is included in the stability field of probertite in the cation–water plane. In the cation–boron systems, however, tertschite, inderite and inderborite are unstable, meyerhofferite, inyoite fall in the stability field of colemanite, and gowerite is metastable phase on the colemanite–ginorite stability line.
2. Common minerals occupy mostly a large stability field, indicating that they can form wide thermodynamic conditions. So they can be found as common borate minerals. On the contrary less common borates can form at very limited thermodynamic conditions seen as activity diagrams with small stability fields, such as ulexite, gowerite and aksaite.
3. Diagrams drawn in the $\log[a_{Mb^{n+}}/(a_{H^+})^n]$ and $\log[a_{Mb^{n+}}/(a_{Mc^{(n-1)+}})(a_{H^+})]$ versus $\log[a_{H_2O}]$ plane, with increasing activity of water, polymerization degree of borates changes from tecto, phyllo, ino, neso borate polyhedra. At the same time $^{[4]}B$ ratio in the structural unit increases with pH, except $\log[a_{Mg^{2+}}/(a_{H^+})^2] - \log[a_{H_2O}]$ diagram.
4. On the contrary, in the diagrams of $\log[a_{Mb^{n+}}/(a_{H^+})^n]$ and $\log[a_{Mb^{n+}}/(a_{Mc^{(n-1)+}})(a_{H^+})]$ versus $\log[a_{B(OH)_3}]$ plane, polymerization degree of borates changes from neso, ino, phyllo, tecto borate polyhedra with increasing activity of $B(OH)_3$.
5. This study showed that why only a few of the naturally occurring borate minerals are common and make deposits and borate associations. Any deposit which borate is primary and which borate is secondary, can be interpreted through activity diagrams, then be verified by textural relations.

Acknowledgments The authors wish to thank Dr. LaMoreaux and an anonymous referee for their constructive reviews and suggestions for the manuscript.

References

Allen RD, Kramer H (1957) Ginorite and sassolite from Death Valley, California. Am Mineral 42:56–61

Alonso RN (1986) Ocurrencia, posicion estratigrafica y genesis de los depositos de borates de la Puna Argentina. PhD desertation, Universitad Nacianal de Salta, Facultad de Ciencias Naturales, Arjantina. Cited in: Smith GI, Medrano MD (eds) (2002) Continental borate deposits of Cenozoic Age. Grew ES, Anovitz LM (eds) Boron, mineralogy, petrology and geochemistry. Reviews in Mineralogy Mineralogical Society of America 33: 263–280

Alonso RN, Gonzales-Barry CE (1995) Geology of Tincalayu (Salta) Borax Deposit. Third Nat Conf Econ Geol 3:A21–A36

Alonso RN, Jordan TE, Tabbutt KT, Vandervoort DS (1991) Giant evaporate belts of the Neogene Central Andes. Geology 19:401–404

Anovitz LM, Hemingway BS (2002) Thermodynamics of boron minerals: summary of structural, volumetric and thermodynamic data. In: Grew ES; Anovitz LM (eds) Boron, mineralogy, petrology and geochemistry, Reviews in Mineralogy, Mineralogical Society of America Washington DC 33, pp 181–265

Barker CE, Barker JM (1985) Borate deposits, Death Valley, California. In: Barker JM, Lefond SJ (eds) Borates: economic geology and production, mining engineering, AIMMPE, pp 103–135, Soc. New York. In: Garrett DE (ed) (1998) Borates, handbook of deposits, processing, properties, and use. Academic Press London, pp 113–181

Barker CE, Wilson JL (1976) Borate deposits in Death Valley region. Guide book: Las Vegas to Death Valley and Return. Nevada Bureau of Mines, Geological Report. 26:22–33. In: Garrett DE (ed) (1998) Borates, handbook of deposits, processing, properties, and use. Academic Press London, pp 113–181

Bernard RM, Kistler RB (1996) Stratigraphic and structural evolution of the Kramer sodium borate ore body, Boron California. In: Rau JL (ed) HE second symposium on salt 1, Northern Ohio Geological Society, pp 133–150

Birsoy R (1990) Stabilities of Ca-, Na-, Mg-, MgCa- and NaCa-borates: application on Turkish deposits. In: Savaşçın MY,

Eronat AH (eds) Proceedings International Earth Sciences Congress on Aegean Regions İzmir, Turkey, pp 222–233
Castor SB (1993) Borates in the Muddy Mountains, Clark County, Nevada. Nevada Bureau of Mines and Geology, Bulletin 107. In: Garrett DE (ed) Borates, handbook of deposits, processing, properties, and use. Academic Press London, pp 113–181
Chandler DC (1996) The Billie Mine, Death Valley, California. In: Garrett DE (ed) Borates, handbook of deposits, processing, properties, and use. Academic Press London, pp 113–181
Christ CL, Clark JR (1977) A crystal-chemical classification of borate structures with emphasis on hydrated borates. Phys Chem Miner 2:59–87
Christ CL, Garrels LM (1959) Relations among sodium borate hydrates at the Kramer deposit, Boron, California. Am J Sci 257:516–528
Christ CL, Truesdell AH, Erd RC (1967) Borate Mineral Assemblages in the System Na_2O-CaO-MgO-B_2O_3-H_2O. Geochem Cosmochim Acta 31:313–337
Countryman RL (1977) Hydroboracite from the Amborgaso Desert, eastern California. In: Garrett DE (ed) (1998) Borates, handbook of deposits, processing, properties and use, Academic Press London. pp 113–181
Evans JR, Taylor GC, Papp JS (1976) Mines and mineral deposits of Death Valley, National Monument, California. In: Garrett DE (ed) Borates, handbook of deposits, processing, properties, and use, Academic Press London, pp 113–181
Foshag W (1921) The origin of the colemanite deposits of California. Econ Geol 16:194–214
Garrels RM, Christ CL (1965) Solutions, minerals and equilibria. Harper and Row, New York, p 450
Garrett DE (1998) Borates, handbook of deposits, processing, properties, and use. Academic Press, London, p 482
Garsia-Veigas J, Rosel L, Orti F, Gündoğan I, Helvacı C (2011) Mineralogy, diagenesis and hydrochemical evolution in probertite-glauberite-halite saline lake (Miocene, Emet Basin, Turkey). Chem Geol 280:352–364
Hawthorne FC, Burns PC, Grice JD (2002) The crystal chemistry of boron. In: Grew ES, Anovitz LM (eds) Boron, mineralogy, petrology and geochemistry, Rev Mineral Mineral Soc Am 33:41–110
Helgeson HC, Delany JM, Nesbitt HW, Bird DK (1978) Summary and the critique of the thermodynamic properties of rock-forming minerals. Am J Sci 278A:229
Helvacı C (1977) Geology, mineralogy and geochemistry of the borate deposits and associated rocks and of the Emet Valley, Turkey, PhD Thesis, University of Nottingham, England, p 338
Helvacı C (1994) Mineral assemblages and formation of the Kestelek and Sultançayırı borate deposits. In: 29th International Geological Congress. Pt. A. pp 245–254
Helvacı C, Alaca O (1991) Geology and Mineralogy of Bigadic Borate Deposits Turkey. Bull Miner Res Explor 113:31–63
Helvacı C, Firman RJ (1976) Geological setting and mineralogy of Emet borate deposits, Turkey. Transact Sect B Inst Min Metall 85:142–152
Helvacı C, Orti F (1998) Sediment logy and diagenesis of Miocene colemanite-ulexite deposits (Western Anatolia, Turkey). J Sed Res 68:1021–1033
Helvacı C, Stamatakis MG, Zagouroglou C, Kanaris J (1993) Borate minerals and related Authigenic silicates in Northeastern Mediterranean Late Miocene Continental Basins. Explor Min Geol 2:171–178
Inan K, Dunham AC, Esson J (1973) Mineralogy, chemistry and origin of Kırka Borate Deposit, Eskisehir Province, Turkey. Inst Min Metall Transact Sect B 82:114–123
Kistler RB, Helvacı C (1994) Boron and Borates. In: Carr DD (ed) Industrial minerals and rocks, society for mining, 6th edn. Metallurgy and Exploration Inc, Littleton, pp 171–186
Kistler RB, Smith WC (1983) Boron and borates. In: Lefond SL (ed) Industrial minerals and rocks, 5th edn. Society of Mining Engineers, New York, pp 533–560
Li J, Li B, Gao S (2000) Calculation of thermodynamic properties of hydrated borates by group contribution method. Phys Chem Mineral 27:342–346
Mattigod SV (1983) A method for estimating the standard free energy of formation of borate minerals. Soil Sci Soc Am J 47:654–655
Meixner H (1965) Borate Deposits of Turkey. MTA Inst Bull Ankara 125:1–12
Orti F, Helvacı C, Rosell L, Gündoğan I (1998) Sulfate-Borate Relations in an Evaporatic Lacustrine Environment: The Sultançayırı Gypsum Member (Miocene, Western Anatolia). Sedimentology 45:697–710
Özpeker I, İnan K (1978) Relations of observed mineral assemblages to the evolution of borate deposits in Western Anatolia. Turkiye Jeoloji Kurumu Bull 21:1–10
Palmer MR, Helvacı C (1995) The boron isotope geochemistry of Neogene borate deposits of Western Turkey. Geochim Cosmochim Acta 61:3161–3169
Schindler M, Hawthorne FC (2001) A bond-valence approach to the structure, chemistry and paragenesis of hydroxyl-hydrated oxysalt minerals. III. Paragenesis of borate minerals. Can Mineral 39:1257–1274
Siefke JW (1991) The boron open pit mine at the Kramer borate deposit: The diversity of mineral and energy resources of southern California. Soc Econ Geol Guideb Ser 12:4–15
Smith GI (1979) Subsurface stratigraphy and geochemistry of late Quaternary evaporates, Searles Lake, California. US Geol Surv Prof Paper 1043:1–130
Smith GI, Medrano MD (2002) Continental Borate Deposits of Cenozoic Age In: Grew ES, d Anovitz LM (eds) Boron, Mineralogy, Petrology and Geochemistry, Reviews in Mineralogy, Mineralogical Society of America Washington DC 33:263–298
Strunz H (1997) Classification of borate minerals. Eur J Mineral 9:225–232
Wagnam DD, Evans HE, Parker VB, Schumm RH, Hallow I, Bailey SM, Churney KL, Nuttall RL (1982) The NBS Tables of Chemical Thermodynamic Properties. Journal of Physical Chemistry Reference Data, 11, National Bureau of Standards Washington DC. p 393
Wendel CA (1978) Special report on borate resources, asupply and marketing study. Mining and minerals Div.National Park Service, US Department of Interior, p 138. Cited in: Smith GI, Medrano MD (eds) (2002) Continental borate deposits of Cenozoic Age. Grew ES, Anovitz LM (eds) Boron, mineralogy, petrology and geochemistry. Reviews in Mineralogy Mineralogical Society of America 33:263–284